Expanded View Figures

Figure EV1. Phylogenetic conservation of Rv1332.

A Pictorial representation of domain architecture of Rv1332.
B Phylogenetic tree depicting actinomycetes encoding for orthologs of Rv1332 (Huerta-Cepas *et al*, 2016).

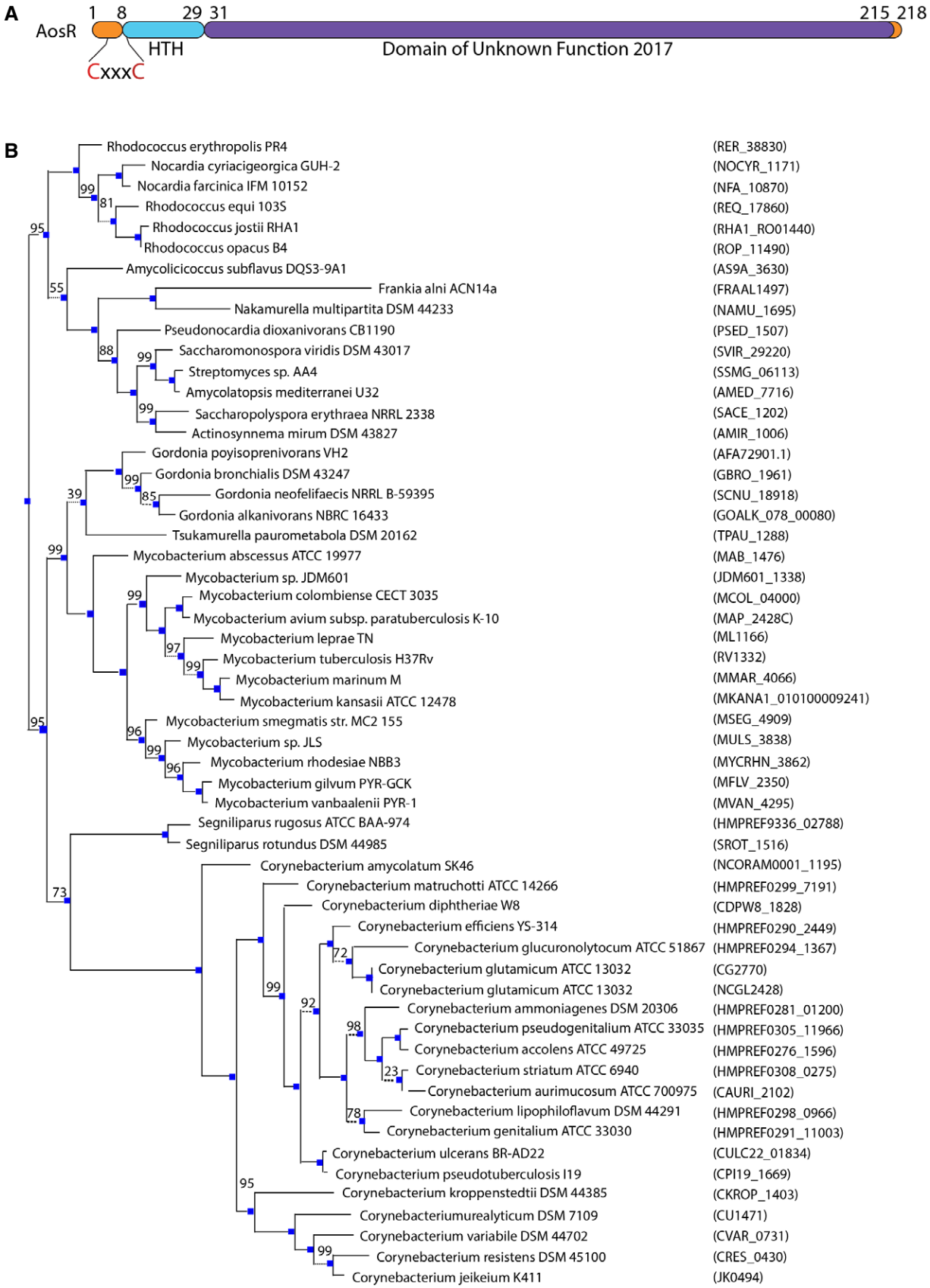
A
AosR
1 8 29 31 215 218
HTH
Domain of Unknown Function 2017
CxxxC
B
Rhodococcus erythropolis PR4 (RER_38830)
Nocardia cyriacigeorgica GUH-2 (NOCYR_1171)
Nocardia farcinica IFM 10152 (NFA_10870)
Rhodococcus equi 103S (REQ_17860)
Rhodococcus jostii RHA1 (RHA1_RO01440)
Rhodococcus opacus B4 (ROP_11490)
Amycolicicoccus subflavus DQS3-9A1 (AS9A_3630)
Frankia alni ACN14a (FRAAL1497)
Nakamurella multipartita DSM 44233 (NAMU_1695)
Pseudonocardia dioxanivorans CB1190 (PSED_1507)
Saccharomonospora viridis DSM 43017 (SVIR_29220)
Streptomyces sp. AA4 (SSMG_06113)
Amycolatopsis mediterranei U32 (AMED_7716)
Saccharopolyspora erythraea NRRL 2338 (SACE_1202)
Actinosynnema mirum DSM 43827 (AMIR_1006)
Gordonia poyisoprenivorans VH2 (AFA72901.1)
Gordonia bronchialis DSM 43247 (GBRO_1961)
Gordonia neofelifaecis NRRL B-59395 (SCNU_18918)
Gordonia alkanivorans NBRC 16433 (GOALK_078_00080)
Tsukamurella paurometabola DSM 20162 (TPAU_1288)
Mycobacterium abscessus ATCC 19977 (MAB_1476)
Mycobacterium sp. JDM601 (JDM601_1338)
Mycobacterium colombiense CECT 3035 (MCOL_04000)
Mycobacterium avium subsp. paratuberculosis K-10 (MAP_2428C)
Mycobacterium leprae TN (ML1166)
Mycobacterium tuberculosis H37Rv (RV1332)
Mycobacterium marinum M (MMAR_4066)
Mycobacterium kansasii ATCC 12478 (MKANA1_010100009241)
Mycobacterium smegmatis str. MC2 155 (MSEG_4909)
Mycobacterium sp. JLS (MULS_3838)
Mycobacterium rhodesiae NBB3 (MYCRHN_3862)
Mycobacterium gilvum PYR-GCK (MFLV_2350)
Mycobacterium vanbaalenii PYR-1 (MVAN_4295)
Segniliparus rugosus ATCC BAA-974 (HMPREF9336_02788)
Segniliparus rotundus DSM 44985 (SROT_1516)
Corynebacterium amycolatum SK46 (NCORAM0001_1195)
Corynebacterium matruchotti ATCC 14266 (HMPREF0299_7191)
Corynebacterium diphtheriae W8 (CDPW8_1828)
Corynebacterium efficiens YS-314 (HMPREF0290_2449)
Corynebacterium glucuronolytocum ATCC 51867 (HMPREF0294_1367)
Corynebacterium glutamicum ATCC 13032 (CG2770)
Corynebacterium glutamicum ATCC 13032 (NCGL2428)
Corynebacterium ammoniagenes DSM 20306 (HMPREF0281_01200)
Corynebacterium pseudogenitalium ATCC 33035 (HMPREF0305_11966)
Corynebacterium accolens ATCC 49725 (HMPREF0276_1596)
Corynebacterium striatum ATCC 6940 (HMPREF0308_0275)
Corynebacterium aurimucosum ATCC 700975 (CAURI_2102)
Corynebacterium lipophiloflavum DSM 44291 (HMPREF0298_0966)
Corynebacterium genitalium ATCC 33030 (HMPREF0291_11003)
Corynebacterium ulcerans BR-AD22 (CULC22_01834)
Corynebacterium pseudotuberculosis I19 (CPI19_1669)
Corynebacterium kroppenstedtii DSM 44385 (CKROP_1403)
Corynebacteriumurealyticum DSM 7109 (CU1471)
Corynebacterium variabile DSM 44702 (CVAR_0731)
Corynebacterium resistens DSM 45100 (CRES_0430)
Corynebacterium jeikeium K411 (JK0494)

Figure EV1.

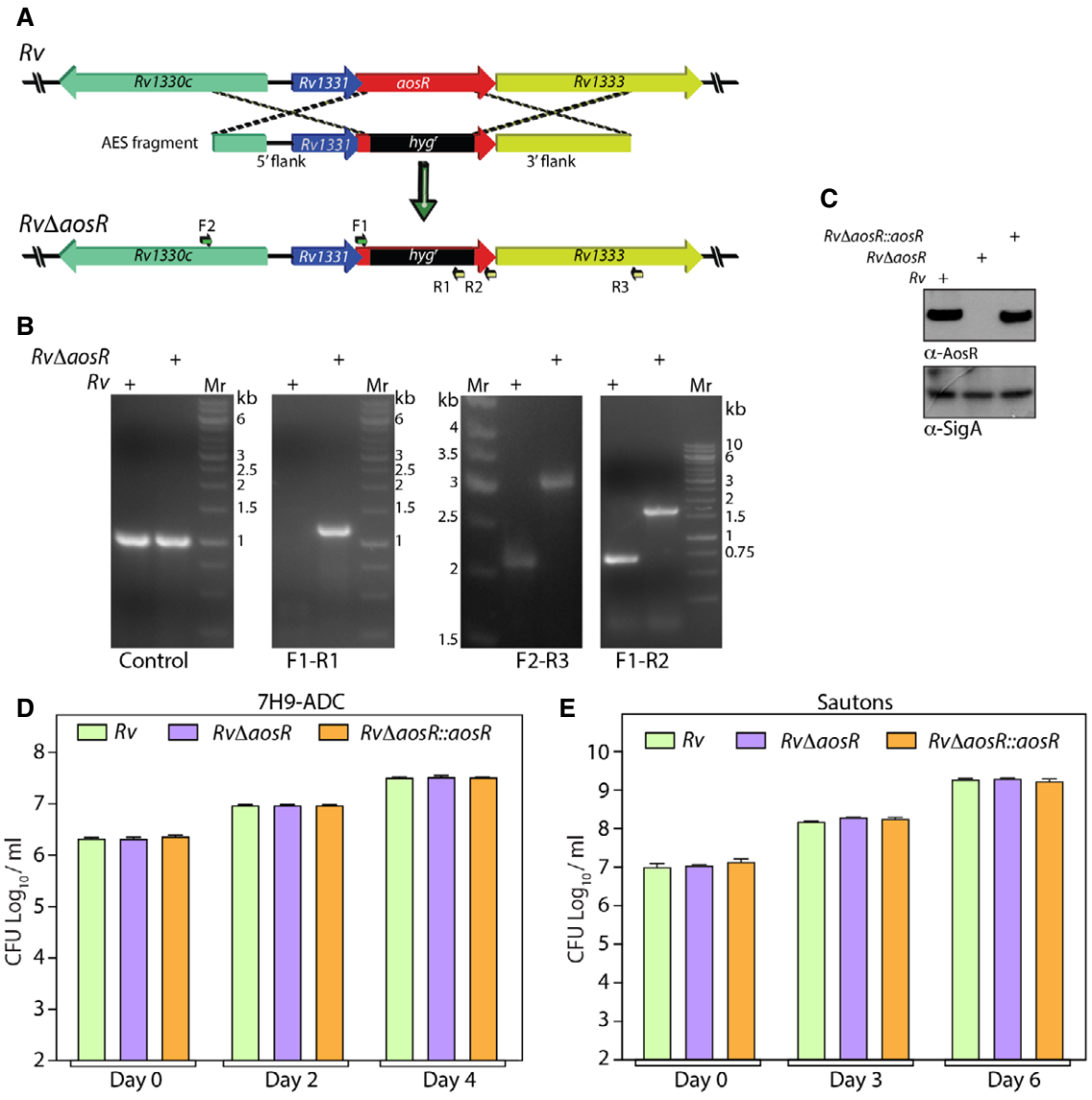

Figure EV2. Generation and characterization of RvΔ1332.

A Schematic representation of loci in *Rv* and *RvΔ1332* strains, depicting replacement *aosR* with *hyg*^{r}. Multiple primer sets used for the PCR-based confirmation are depicted.

B PCR amplicons from *Rv* and *RvΔaosR* were resolved on 1% agarose gels. Primer pairs used for the amplification are indicated. First panel (control): ~ 0.97 kb amplicons of *sigB* in both the strains. The second panel shows amplicons (~ 1.2 kb) obtained only in *RvΔ1332*. The third panel shows differential amplicon sizes with primers beyond AES in *Rv* (~ 2.1 kb) and *RvΔ1332* (~ 3.1 kb) to confirm site-specific recombination, and fourth panel shows differential amplification of *Rv1332* gene in *Rv* (0.67 kb) and *RvΔaosR* (1.6 kb). Mr represents molecular marker.

C 35 μg WCLs prepared from *Rv*, *RvΔaosR*, and *RvΔaosR::aosR* were resolved on 15% SDS–PAGE, transferred to nitrocellulose membrane, and probed with α-AosR and α-SigA antibodies.

D, E Logarithmic phase cultures of *Rv*, *RvΔaosR*, and *RvΔaosR::aosR* were inoculated at (D) A_{600} ~ 0.05 in 7H9-ADC and CFU (mean ± SEM; n = 3) were enumerated at days 0, 2, and 4 or (E) at A_{600}~0.01 in Sauton's media and CFU (mean ± SEM; n = 3) were enumerated at days 0, 3, and 6.

Source data are available online for this figure.

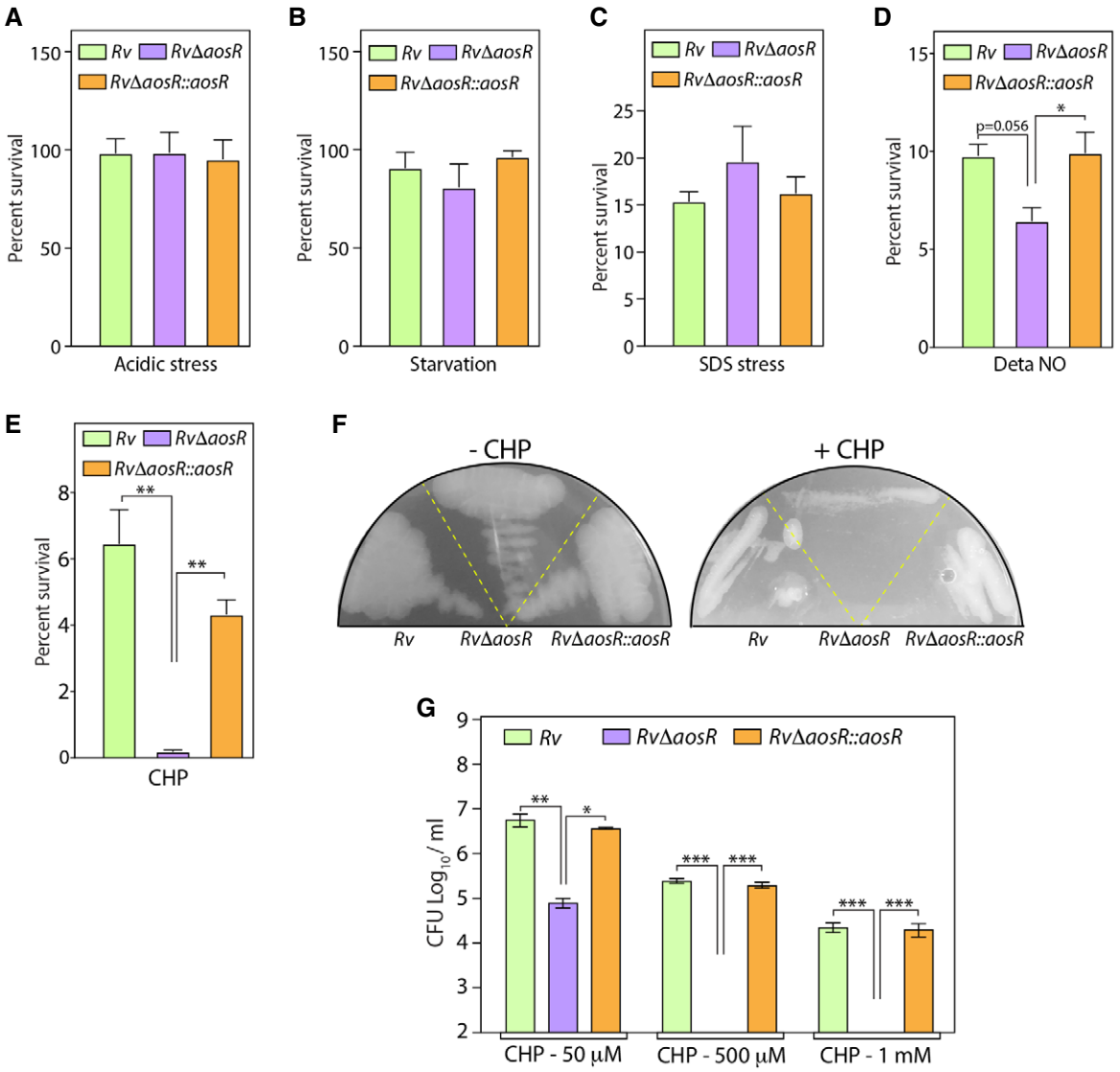

Figure EV3. AosR specifically mitigates oxidative stress.

A To assay the sensitivity of *Mtb* strains to acidic stress, single-cell suspensions of *Rv*, *RvΔaosR*, and *RvΔaosR::aosR* were inoculated in 7H9-ADC acidified to pH 4.5 and CFUs were enumerated after a week ($n = 3$).

B Early-log-phase culture of *Rv*, *RvΔaosR*, and *RvΔaosR::aosR* was washed and resuspended in PBS containing 0.1% Tween 80 at $A_{600} \sim 0.3$. Bacterial survival was examined after a week ($n = 3$).

C For surfactant stress, mid-logarithmic phase bacterial cultures were grown in 7H9-ADC broth containing 0.1% SDS for 3 h, and CFUs were enumerated ($n = 3$).

D, E Logarithmic phase bacterial strains were inoculated at $A_{600} \sim 0.3$ in 7H9-ADS (D) containing 1 mM DETA-NO for 2 days or (E) 50 μM CHP for 24 h ($n = 3$).

F Bacterial strains inoculated at $A_{600} \sim 0.2$ in the presence or absence of 50 μM CHP for 24 h were streaked on 7H11-OADS plates.

G Logarithmic phase bacterial strains were treated with increasing indicated concentrations of CHP for 24 h. The data depicts mean ± SEM, representative of two independent experiments performed in triplicates.

Data information: (A–E) CFU obtained at day 0 was set as 100%, and percent survival was calculated. Data are plotted as mean percent survival (± SEM). Statistical significance was analyzed using one-way ANOVA followed by *post hoc* test (Tukey test; GraphPad prism). *$P < 0.05$; **$P < 0.005$; and ***$P < 0.005$.

Source data are available online for this figure.

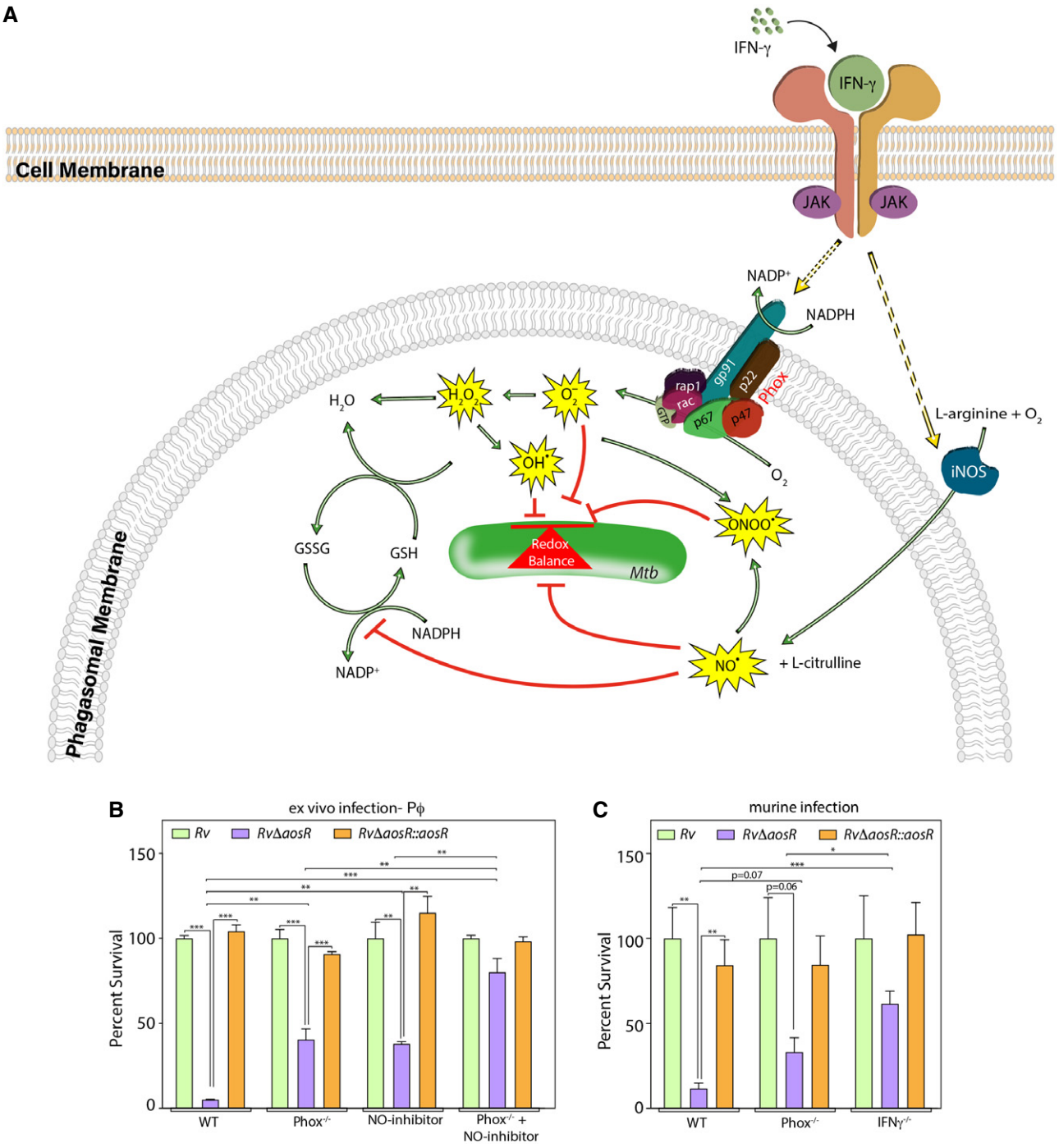

Figure EV4. Pathways of ROS production and degradation.

A NADPH phagocyte oxidase (phox) activity is enhanced by IFNγ. It reduces oxygen (O_2) to superoxide ($O_2^{\bullet -}$), which can either react with nitric oxide to generate peroxynitrite ($ONOO^-$) or be converted to less reactive species hydrogen peroxide (H_2O_2) by superoxide dismutase. H_2O_2 is either reduced to water by catalase or glutathione reaction or react with Fe^{2+} to form highly potent hydroxyl radicals ($HO^{\bullet}$) via Fenton reaction. Generation of $O_2^{\bullet -}$ is additionally contributed by xanthine oxidase, mitochondria, and uncoupled nitric oxide synthase.

B CFU obtained for *Rv* in each set (Fig 2D) was normalized to 100%, and mean percent survival ± SEM (n = 3) of *RvΔaosR* and *RvΔaosR::aosR* was calculated.

C CFU obtained for *Rv* in each mice strain (Fig 2E) was normalized to 100%, and mean percent survival ± SEM (n = 3) of *RvΔaosR* and *RvΔaosR::aosR* was calculated.

Data information: Statistical significance was analyzed using one-way ANOVA followed by a *post hoc* test (Tukey test; GraphPad prism).
Source data are available online for this figure.

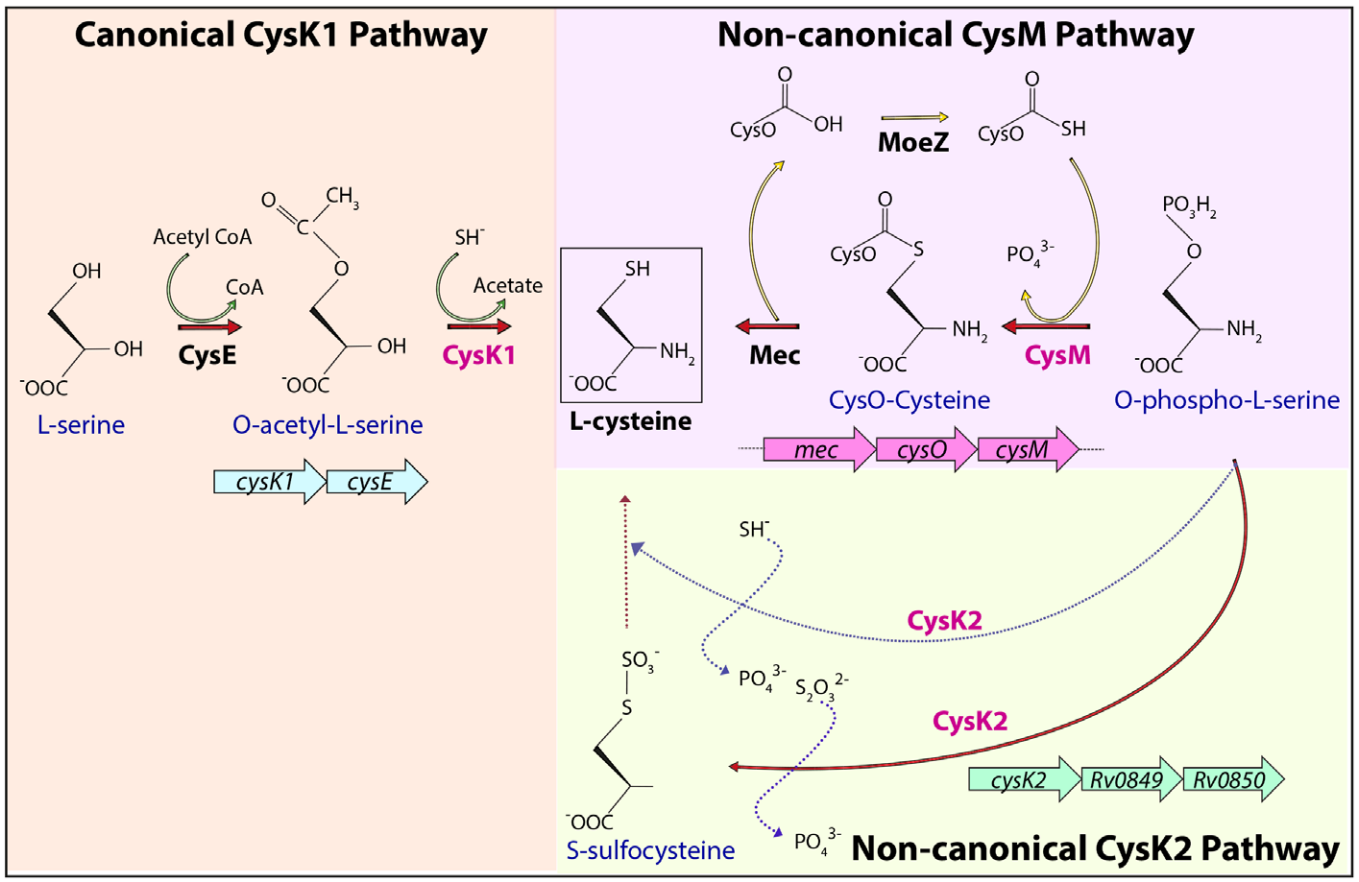

Figure EV5. Cysteine biosynthesis pathways in *Mtb*.

There are three *de novo* cysteine biosynthesis pathways in *Mtb*. The canonical cysteine synthase CysK1 utilizes O-acetyl-L-serine derived from serine and sulfide derived from the reductive branch of APS pathway as substrates. CysM pathway is unique to actinomycetes and uses O-phospho-L-serine as acceptor substrate and thiocarboxylated CysO as a sulfur donor. CysK2 pathway generates either L-cysteine when sulfide is used or S-sulfocysteine when thiosulfide is used. The latter can be reduced to L-cysteine or used as an oxidative stress response-signaling molecule.